Available online at www.sciencedirect.com
SCIENCE DIRECT®

Journal of the European Ceramic Society 23 (2003) 1305–1311

www.elsevier.com/locate/jeurceramsoc

Microstructural changes of processed vitrified solid waste products

P. Kavouras, Ph. Komninou*, K. Chrissafis, G. Kaimakamis, S. Kokkou, K. Paraskevopoulos, Th. Karakostas

Physics Department, Aristotle University, 541 24 Thessaloniki, Greece

Received 29 March 2002; received in revised form 26 July 2002; accepted 7 August 2002

Abstract

Toxic lead-rich solid industrial wastes were stabilized by the vitrification method. Vitrification was attained by the addition of SiO_2 and Na_2O as vitrifying and melting agent, respectively. The non-toxic, homogeneous, vitreous products studied in the present work, contain 60 wt.% of solid waste. Products with such a high content of solid waste comprise an economically realistic suggestion, but are easily devitrified in conditions of large-scale production due to the difficulty to achieve rapid cooling conditions in the whole volume of a large piece of stabilized product. Thus, it must be ascertained that the loss of homogeneity is not accompanied with the loss of chemical stability. Differential Thermal Analysis (DTA) was applied in order to inspect the prospect to crystal phase separation. The separated crystal phases were characterized by X-ray diffraction and transmission electron microscopy. Possible devitrification processes are investigated in order to interconnect the microstructure with the chemical stability of the devitrified products.

Keywords: Devitrification; Electron microscopy; Glass ceramics; Vitrification; Wastes

1. Introduction

The vitrification method has been proved to be one of the most promising and low-cost methods for the stabilization of hazardous solid wastes and it has been applied for the stabilization of a variety of urban,[1] industrial[2,3] and radioactive[4,5] waste forms. Furthermore, the vitrification process usually results in a large waste volume reduction, with evident benefits in terms of storage or dumping.[3] It comprises of the co-melting of the solid waste with appropriate vitrifying and melting agents. The toxic elements and/or chemical substances can either participate on the formation of the glass network or be captivated in the form of precipitates or crystal phases in the glass network. In all cases, they are entrapped on the volume of the vitreous product and become chemically inactive. The large-scale implementation of this method requires low cost vitrifying and melting agents, a sufficiently high waste content and pour temperatures easily attainable from a commercial furnace.

The vitrification method was applied for the stabilization of a rich in lead and iron oxides solid waste (ash) that originates from the combustion of sludge recovered from storage tanks of tetraethyl lead (TEL) and leaded gasoline. This solid waste was successfully stabilized by the addition of the appropriate vitrifying agents in various proportions. The highest content of solid waste, efficient for the synthesis of a non-toxic vitreous product, was found to be 60 wt.%.[6] Compositions with high iron content exhibit a tendency for spontaneous crystallization;[7] consequently, in large-scale applications the presence of such a high waste content in a stabilized homogeneous vitreous product can give rise to crystal phase separation or, as it is usually referred, devitrification during the cooling stage. The conditions for devitrification can occur, in large-scale production, during the slow cooling in the interior of large pieces of stabilized vitreous products, since when they are subjected to quenching, only a surface layer will be rapidly cooled down. The interior of the products will be separated in shells of continuously lower cooling rate, due to the low thermal conductivity of the glass. As a result, the interior volume will partially crystallize.

The devitrification process can alter the composition of the amorphous matrix and as a result its chemical

* Corresponding author: Tel.: +30-310-99-81-95; fax: +30-310-99-80-61.

E-mail address: komnhnoy@auth.gr (P. Komninou).

0955-2219/03/$ - see front matter © 2002 Elsevier Science Ltd. All rights reserved.
PII: S0955-2219(02)00289-3

resistance. Additionally, the separated crystal phases can be leached away from the matrix and constitute a potential environmental danger. In order to simulate such a process, a vitrified product synthesized in the laboratory scale was subjected to a number of annealing processes based on the results of Differential Thermal Analysis (DTA) that revealed all possible crystallization processes responsible for devitrification.

This work is focused on the understanding of the possible devitrification mechanisms leading to a heterogeneous, multicomponent and multiphase material, the microstructural characterization of the different separated crystal phases and the connection of their microstructure with the chemical or environmental stability of the devitrified product. The results can be used as a guide for the most appropriate application of the stabilized products.

2. Experimental

The initial solid waste (ash) was in powder form and it was produced from the incineration of sludge recovered from storage tanks of tetraethyl lead (TEL) and leaded gasoline. The ash was co-melted with quantities of SiO_2 and Na_2CO_3 powders in a platinum crucible. The melt was poured from 1400 °C and quenched on a stainless steel plate at ambient atmosphere and temperature. A detailed presentation of the methods used to assess the chemical composition of the ash can be found elsewhere.[6]

DTA curves were obtained with a Setaram TG DTA SetSys 1750 °C instrument in Argon atmosphere for three types of samples: (a) as-quenched and (b) thermally pretreated-both in powder form- and (c) as-quenched bulk. Thermally pretreated samples were obtained from as-quenched by heating at 950 °C. All DTA scans were comprised of a heating stage, until the temperature of 950 °C, followed by a cooling stage until room temperature, both with a constant temperature gradient of 10 °C/min. The annealing processes were composed of a heating stage, until the desired temperature, with a constant rate of 10 °C/min, followed by an isothermal heating of half an hour, at the maximum obtained temperature. The samples that were annealed were in the form of solidified droplets of 1 cm in diameter. The annealed samples were morphologically characterized with a Zeiss Axiolab-α optical metallographic microscope and a JEOL JSM-840A Scanning Electron microscope. All morphological characterizations were conducted on flat and mechanically polished sections of the vitrified samples. Additionally, the elemental composition of the matrix and of the crystallites responsible for devitrification was studied with an OXFORD ISIS-300 EDS analyzer.

Structural characterization was performed by the X-Ray Diffraction technique (XRD) with a Seifert 3003 powder diffractometer, utilizing CuKα1 radiation. TEM observations were carried out using a JEOL JEM-120CX and a JEOL JEM-2010 electron microscopes, operated at 120 and 200 kV respectively, the latter equipped with a Link EDS microanalyzer capable of analyzing particles of a few nanometers in size. Specimens for TEM investigations were prepared by standard mechanical grinding, followed by chemical final thinning in an appropriate bath (5% HF, 10% HCl, 85% H_2O).

3. Results

3.1. Initial ash—vitrification product

The elemental and chemical composition of the solid waste is presented in Table 1. The vitrified product composed of 60% solid waste, 25% SiO_2 and 15% Na_2O weight percent. The homogeneity of the vitrified product, prior to any thermal processing, was examined by doing several EDS analyses on different locations in different polished sections. The standard deviations of the measurements concerning all batch elements were in the order of ±1%, which is comparable with the sensitivity of the method. These were the first results that suggested the production of a homogeneous product without any crystal phase separation. Additionally, the homogeneity was also recognized upon optical inspection using a metallographic microscope.

3.2. DTA results

DTA heating curves are depicted in Fig. 1. Curve (a) of the powder sample contains a well-defined glass transition point at ≈440 °C followed by a hysteresis. Peaks (1) and (2) represent the devitrification process that occurs in two steps, namely by two crystallization processes positioned at 600 and 800 °C respectively. The above were verified with the aid of XRD experiments that will be presented below. The curve of the previously heat-treated sample (b) does not contain any crystallization peak. The only discrete characteristic is the glass transition point. The absence of crystallization

Table 1
Chemical and elemental composition of the incinerated sludge (ash)

Compound	Wt.%	Elements	Wt.%
Fe_2O_3	47.3	Fe	33
$PbO{\cdot}PbBr_2$	37.4	Pb	29.6
$PbSO_4$	2.3	Br	10.1
PbO	2.0	Si	1
SiO_2	2.2	S	0.25
Al_2O_3	1.5	Al	0.8
Other oxides	3.3	Sb	0.3
Moisture	4.0	–	–

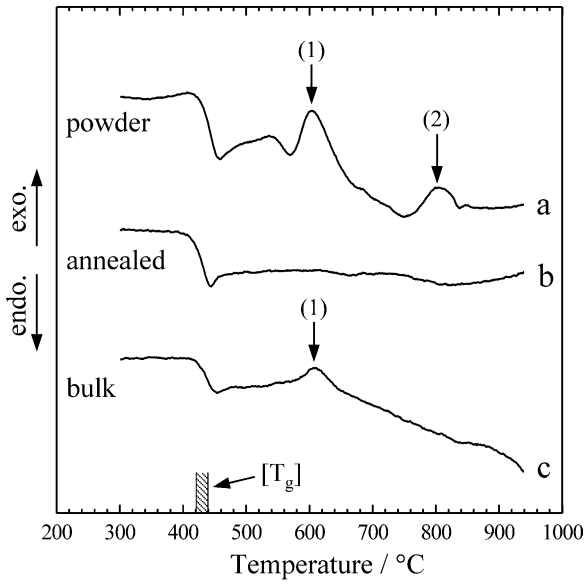

Fig. 1. DTA scans curves (a), (b) and (c) correspond to the as-quenched powder, previously heat-treated powder and as-quenched bulk samples respectively.

peaks can be attributed to the fact that the previously heat-treated sample has already been crystallized and as a result has been transformed into a more stable state, which is not susceptible to further devitrification.

The position of the glass transition temperature (T_g) does not lie on a specific point, but its value rather lies on a temperature range of $\sim$10 °C, namely on a transformation interval of [T_g] = 430–440 °C, as it is indicated in Fig. 1 by the dashed column. The fact that the cooling rate from the melt is possibly not entirely constant between all vitrified samples (e.g. melt drops of a different mass will be cooled down in slightly different rates), can give rise to a slight variation of the glass transition point.[8]

A different DTA scan (curve c) is presented in Fig. 1, concerning the as-quenched bulk sample. Since the bulk sample, which possesses less specific area, did not produce peak (2), it can be reasonably assumed that the corresponding crystallization takes place on a surface layer. The origin of this crystallization is possibly a heterogeneous surface nucleation of the specific crystal phase. This assumption will be supported from the morphological observations, which will be presented below. Additionally, crystallization peak (1) is present in both samples. In other words, the first step of the devitrification process possibly originates from the interior of the sample in a manner similar to homogeneous nucleation.

3.3. Morphological and XRD results

In order to characterize the crystalline phases responsible for the crystallization peaks (1) and (2) obtained in the DTA scans, three annealing processes were carried out that lie just before the beginning of peak (1), between peaks (1) and (2) and after every phase separation: at 560, at 720 and at 900 °C, respectively.

The XRD diffractograms are presented in Fig. 2, together with that of the as-quenched sample. The diffractogram that corresponds to the as-quenched sample (a) suggests that it is mainly composed of an amorphous matrix while the appearance of two faint peaks that correspond to Hematite, suggests the presence of a small proportion of this phase in microcrystalline form. After annealing at 560 °C the peaks of Hematite increase in intensity, since crystal growth should have occurred. Additionally, a new faint peak that corresponds to Magnetoplumbite ($PbFe_{12}O_{19}$) begins to be present. At 720 °C the peaks of Hematite are more intense as well as those of Magnetoplumbite. Taking into account the above arguments, the peak at 600 °C in the DTA thermogram should be connected with the nucleation of the crystal phase of Magnetoplumbite and the growth of Hematite that is already found in the as-quenched sample (diffractogram a). Additionally, the difference between diffractograms a and b should be attributed to the isothermal part of the annealing process and not to crystal growth or nucleation that took place between [T_g] and 560 °C.

After annealing at 900 °C the initially vitreous product has been intensively crystallized, since both Hematite and Magnetoplumbite crystals have grown into the amorphous matrix but no other crystalline phase was detected. According to the above analysis, the origin of DTA peak (2) could be attributed to the growth of Hematite and Magnetoplumbite. The fact that peak (2) is not present in the bulk sample led to the application of the same annealing steps in pulverized vitreous products. As it is depicted in diffractogram (e), the only crystal phase that has grown in the amorphous matrix is Hematite. Consequently, DTA peak (2) that is present

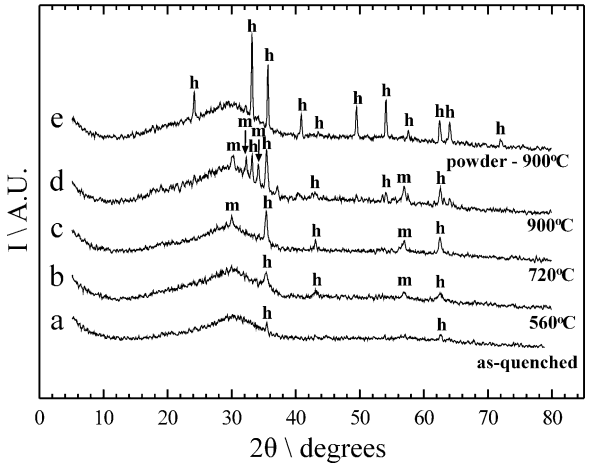

Fig. 2. X-ray diffractograms, corresponding to (a) as-quenched vitreous product, bulk samples annealed at (b) 560 °C, (c) 720 °C, (d) 900 °C and (e) sample in powder form annealed at 900 °C.

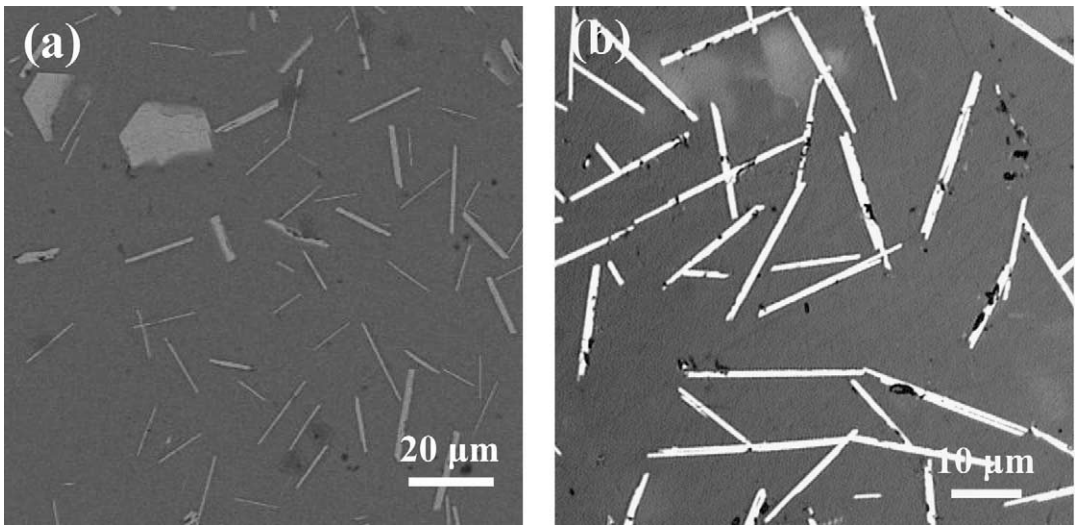

Fig. 3. Optical micrographs of devitrified (a) bulk and (b) powder product after annealing at 900 °C.

only in the powder sample, could be associated to the surface heterogeneous nucleation and growth of Hematite. As a result, the Hematite in the powder sample annealed at 900 °C originates from two different processes: (i) from the growth of the existing nuclei in the as-quenched sample that is indicated from the peak (1) of the DTA scan (a); and (ii) from the surface nucleation of Hematite, indicated from peak (2) of the same DTA scan.

Morphological studies, conducted in all the bulk samples annealed at 720 and 900 °C, illustrated the existence of the two crystalline phases separated from the matrix. Two characteristic optical micrographs obtained from mechanically polished sections are depicted in Fig. 3. EDS analyses revealed that the hexagonal crystallites (Fig. 3a) that were grown after annealing at 900 °C posses a Fe/Pb atomic ratio of 12, compatible with Magnetoplumbite, while the needle like ones contain only Fe and O with an atomic ratio of Fe/O close to 2/3, corresponding to Hematite; therefore, the EDS analyses support XRD results. It must be pointed out that some of the hexagonal crystallites can appear as needles too, since they are hexagonal foils. For this reason their morphology depends on the angle that they intersect the polished section of the sample. The morphology of the powder sample that was annealed at 900 °C is different in the sense that all hexagonal crystallites are absent. Only needle-like Hematite crystallites are present as it is depicted in Fig. 3b.

In Fig. 4 three droplets of the vitrified product annealed at 900 °C, are illustrated. These droplets were softened and consolidated, since the annealing temperature is well beyond the glass transition region. Thus, their surfaces can be clearly distinguished only due to the surface nucleation of the needle-like crystallites. From this micrograph it can be verified that the needle-like crystallites start growing at the surface of the specimen and they impinge to a depth of not more than ≈70 μm. This could be the reason why the corresponding crystallization peak, located at 800 °C, is present only in the DTA curve of the powder and not on the bulk sample.

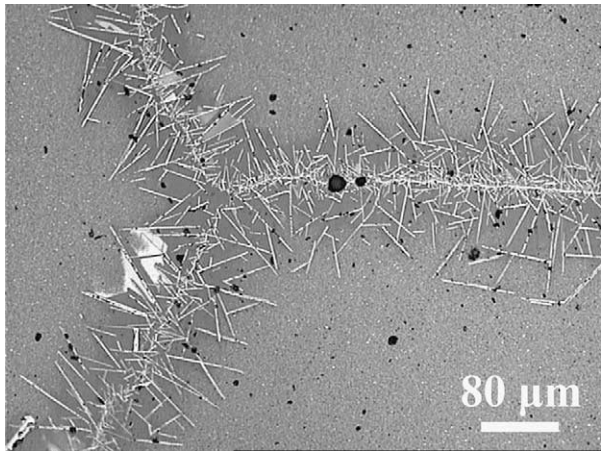

Fig. 4. Optical micrograph of the interface of three droplets of as-quenched vitrified product after annealing at 900 °C for 30 min. The Hematite needle-like crystallites impinge from the surface reaching a depth of approximately 70 μm.

3.4. TEM results

TEM micrographs of the product annealed at 720 °C show the Magnetoplumbite crystallites; they have almost perfectly hexagonal morphology as it is illustrated in Fig. 5. Diffraction pattern (a) was obtained with the electron beam parallel to the [0001] zone axis, while (b) was taken along the [01$\bar{1}$0] zone axis, after tilting the specimen. The analysis of the diffraction patterns confirmed beyond any doubt that such hexagonal

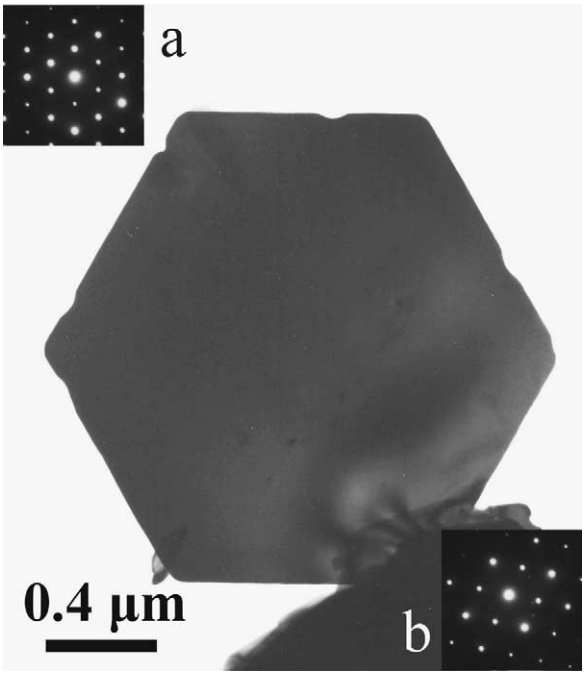

Fig. 5. A hexagonal Magnetoplumbite crystallite viewed along the [0001] zone axis. The two inserted diffraction patterns were taken along (a) [0001] and (b) [01$\bar{1}$0] zone axes.

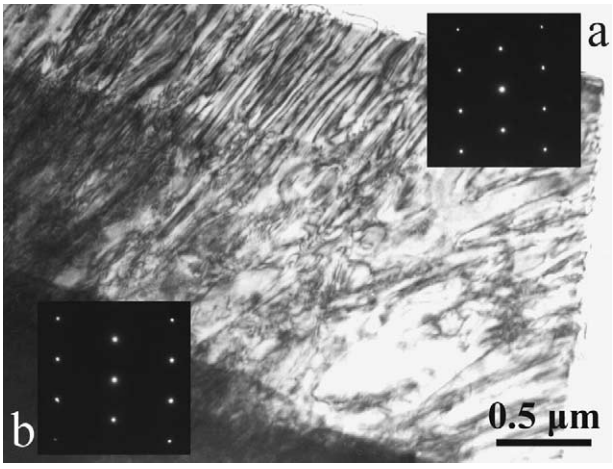

Fig. 6. A Hematite crystallite observed in the powder specimen that was annealed at 900 °C. The two inserted diffraction patterns (a) and (b) were obtained parallel to the [1$\bar{2}$1$\bar{3}$] and [$\bar{2}$4$\bar{2}$3] zone axes, respectively.

crystallites are Magnetoplumbite crystallites. Magnetoplumbite crystallizes to the $P6_3/mmc$ space group with lattice parameters $a = 5.873$ Å and $c = 23.007$ Å. Their morphology is characteristic of their hexagonal symmetry and consistent with the observation that their nucleation took place in the interior of the product.

A characteristic Hematite crystallite that was grown from surface heterogeneous nucleation is presented in Fig. 6, together with two diffraction patterns. Diffraction patterns (a) and (b) were obtained with the electron beam parallel to the [1$\bar{2}$1$\bar{3}$] and [$\bar{2}$4$\bar{2}$3] zone axes, respectively. The analysis of the diffraction patterns confirmed that such crystallites are Hematite crystallites. The reason that they appear as needles is that are extended foils cut in an arbitrary angle with respect to their plane. Hexagonal Hematite crystallizes to the P3 space group having lattice parameters $a = 5.56$ Å and $c = 22.55$ Å.

4. Discussion

A vitreous product was produced containing satisfactorily high percentage of a toxic solid waste. It must be pointed out that the specific solid waste contains significantly higher lead component (Table 1) compared to common sludge of the same origin; a typical lead content is in the order of 1–2% (wt.). The leach resistance was found to be sufficient,[6] according to the limits of USEPA. In the same reference is also reported that annealing at temperatures of crystal phase separation, affects leaching resistance. After crystallization of Magnetoplumbite the product becomes more chemically resistant, while nucleation of Hematite creates a product with a significantly weaker leaching resistance comparable to that of the initial solid waste. As a result, leach resistance is strongly affected from the microstructure of the initially vitrified product. In order to interpret the ability to synthesize a vitreous product with such a composition (relatively low concentration in SiO_2 that is the main glass former), on the first place, and the strong effect of the devitrification in the leach resistance, on the second place, the structural role of the main oxides should be taken into consideration.

Considering the relatively high concentration of the Na_2O that constitutes a glass modifier[9] and acts as a melting agent by breaking some of the Si–O–Si linkages, the creation of a vitreous network that was verified by XRD, is somewhat contradictory. This is also supported from the fact that the Si/O ratio is too low; namely, Si/O = 0.25. As it is well established, a vitreous network can be formed for a Si/O ratio in the range of 0.33.[2] For Si/O values smaller from 0.33 the network obtained is not polymerized and it consists of chains made up of a few polyhedra or isolated polyhedra, depending on the deviation from the above number. The aforementioned lead to the assumption that one component of the ash should be able to act as a glass former. In the present case, PbO cannot act in such way, since it is found in low concentration. It has been reported in the literature that PbO can form a glass network only when it is found in high concentrations (namely, higher than 40–60 mol%).[10–12]

On the other hand, Fe_2O_3 that is found in large quantities in the initial ash is a serious candidate to take part in the construction of the vitreous network of the stabilized product. It has been found that Fe_2O_3 can be

incorporated into a sodium silicate glass and increase the number of polyhedra taking part in the vitreous network.[13] It can thus act as an intermediate rather than a modifier, in contrast to Fe^{2+} that is a modifier. The degree of reduction of Fe^{3+} to Fe^{2+} during glass melting is higher for Fe_2O_3 concentration lower than 5 mol%. Since Fe_2O_3 batch concentration is 20 mol%, higher than the above value, it is expected that Fe^{3+} is the dominant species in the high Fe_2O_3 content of sodium silicate glasses.[13,14]

As it is mentioned above, the crystallization of Magnetoplumbite ($PbFe_{12}O_{19}$) led to a more chemically stable product, while crystallization of Hematite resulted to a detrimental increase of lead content in the leachate. The above results can be explained, through the previous analysis of the structural role of the main oxides contained in the vitrified solid wastes. In the case of Magnetoplumbite, the separated phase contains lead; as a result the matrix was depleted from a part of this element's content. Consequently, this caused a reduced concentration of lead in the leachate. On the other hand, the lead content of the separated crystalline phase is strongly bonded inside the structure of Magnetoplumbite and in that way lead seems to become non-leachable.

On the contrary, the surface crystallization of Hematite removed a significant part of Fe^{3+} ions and at the same time prohibited the nucleation of Magnetoplumbite. In this way, the matrix became enriched in Fe^{2+} and Pb^{2+} ions that, as it was mentioned above, both constitute glass modifiers. Although the surface crystallization of Hematite has been reported in other studies as a result of the surface oxidation of Fe^{2+} to Fe^{3+},[7,15,16] the depletion of the Fe^{2+} ions will be localized in a narrow surface layer. When the Hematite crystallites impinge towards the interior of the vitrified product, where oxygen from the atmosphere is absent, Fe^{3+} ions will be removed from the matrix for the evolution of the growth process that was observed by optical microscopy. This results in a higher content in non-bridging oxygen in the volume of the matrix, leading to a weaker network insufficient to captivate lead. In that way it is possible that the surface nucleation of Hematite produced a detrimental alteration of the leach resistance.

5. Conclusion

A stabilized solid waste, with a 60% weight ratio waste content, was produced using the vitrification process. The lead rich solid waste was vitrified by the addition of SiO_2 and Na_2O. DTA measurements were obtained for both as-quenched and previously heat treated samples. Heating scans operated on pulverized and monolithic as-quenched samples showed one exothermic peak at 600 °C that is common in both samples and another at 800 °C that is present only in the powder samples. The DTA traces of the previously heat-treated samples did not produce crystallization peaks, as it was expected. The position of the glass transition temperature of the aforementioned samples was detected to lie on the same temperature range of ~10 °C, namely on a transformation interval of $[T_g] = 430$–440 °C.

Annealing processes performed in temperatures indicated from the position of the DTA crystallization peaks, gave rise to the growth of crystal phases responsible for devitrification. The phase of Magnetoplumbite ($PbFe_{12}O_{19}$) nucleates and grows as one of the dominant crystal phases together with Hematite, as it was determined from XRD and TEM studies, performed on the samples annealed at 720 °C. The growth of Magnetoplumbite enhances the chemical stability, while above 800 °C the heterogeneous surface nucleation of Hematite drastically deteriorates it.

Conclusively, a large piece of a vitrified waste will not be homogeneous, since the cooling rate will continuously decrease while getting away from the surface. Except from an as-quenched homogeneous region near the surface, the interior of a large piece will, apparently, undergo devitrification. Consequently, the chemical stability will be further increased in the volume where Magnetoplumbite is separated, while it will be drastically reduced where Hematite will nucleate. Even though a large volume of product would not have a large specific area, the heterogeneous nucleation of Hematite could be initiated on the surface of foreign particles that had been secluded in the batch materials. As a result, the interior of the product will be inhomogeneous, with respect to its chemical stability.

This kind of final product can be appropriate for safe disposal of the ash, since its inhomogeneous interior is covered by a chemically resistant amorphous crust. However, it cannot be crushed to produce, for example, road stones because some of the potentially weakened matrix regions will be exposed to the environmental influence, except if it can be produced in the form of gravels from the pour stage.

References

1. Romero, M., Rawlings, R. D. and Rincón, J. Ma., Development of a new glass-ceramic by means of controlled vitrification and crystallisation of inorganic wastes from urban incineration. *J. Eur. Ceram. Soc.*, 1999, **19**, 2049–2058.
2. Pisciella, P., Crisucci, S., Karamanov, A. and Pelino, M., Chemical durability of glasses obtained by vitrification of industrial wastes. *Waste Manag. (N.Y.)*, 2001, **21**, 1–9.
3. Scarinci, G., Brusatin, G., Barbieri, L., Corradi, A., Lancellotti, I., Colombo, P., Hreglich, S. and Dall'Igna, R., Vitrification of industrial and natural wastes with production of glass fibres. *J. Eur. Ceram. Soc.*, 2000, **20**, 2485–2490.
4. Sheng, J., Vitrification of borate waste from nuclear power plant

using coal fly ash. (II) Leaching behavior of the FA30 glass. *Fuel*, 2002, **81**, 253–256.
5. Chin-Ching Tzeng, Yung-Yen Kuo, Tsair-Fuh Huang, Deng-Lain Lin and Yuh-Jenq Yu, Treatment of radioactive wastes by plasma incineration and vitrification for final disposal. *J. Hazard. Mater*., 1998, **58**, 207–220.
6. Kavouras, P., Kaimakamis, G., Ioannidis, Th. A., Kehagias, Th., Komninou, Ph., Kokkou, S., Pavlidou, E., Antonopoulos, I., Sofoniou, M., Zouboulis, A., Hadjiantoniou, C. P., Prakouras, A. and Karakostas, Th., *Waste Management* (in press).
7. Karamanov, A. and Pelino, M., Crystallization phenomena in iron-rich glasses. *J. Non-Cryst. Sol*., 2001, **281**, 139–151.
8. Zarzycki, J., *Glasses and the Vitreous State*. Cambridge University Press, 1991.
9. Zotov, N., Effects of composition on the vibrational properties of sodium silicate glasses. *J. Non-Cryst. Sol*., 2001, **287**, 231–236.
10. Wang, P. W. and Zhang, L., Structural role of lead in lead silicate glasses derived from XPS spectra. *J. Non-Cryst. Sol*., 1996, **194**, 129–134.
11. Fayon, F., Landron, C., Sakurai, K., Bessada, C. and Massiot, D., Pb^{2+} environment in lead silicate glasses by Pb-L_{III} edge XAFS and ^{207}Pb NMR. *J. Non-Cryst. Sol*., 1999, **243**, 39–44.
12. Fayon, F., Bessada, C., Massiot, D., Farnan, I. and Coutures, J. P., ^{29}Si and ^{207}Pb NMR study of local order in lead silicate glasses. *J. Non-Cryst. Sol*., 1998, **232–234**, 403–404.
13. Holland, D., Mekki, A., Gee, I. A., McConville, C. F., Johnson, J. A., Johnson, C. E., Appleyard, P. and Thomas, M., The structure of sodium iron silicate glass—a multi-technique approach. *J. Non-Cryst. Sol*., 1999, **253**, 192–202.
14. Mekki, A., Holland, D., McConville, C. F. and Salim, M., An XPS study of iron sodium silicate glass surfaces. *J. Non-Cryst. Sol*., 1996, **208**, 267–276.
15. Karamanov, A., Pisciella, P. and Pelino, M., The crystallization kinetics of iron rich glass in different atmospheres. *J. Eur. Ceram. Soc*., 2000, **20**, 2233–2237.
16. Karamanov, A., Taglieri, G. and Pelino, M., Iron-rich sintered glass-ceramics from industrial wastes. *J. Am. Ceram. Soc*., 1999, **82**, 3012–3016.